IJASS
International Journal of
Aeronautical and Space Science

Vision-Based Relative State Estimation Using the Unscented Kalman Filter

Daero Lee*

Postdoctoral Research Associate, Wind Power Grid-Adaptive Technology Research Center, Chonbuk National University, Jeonju, 560-756, Korea

Henry Pernicka**

Associate Professor, Missouri University of Science & Technology, Rolla, Missouri 65409-0050, USA

Abstract

A new approach for spacecraft absolute attitude estimation based on the unscented Kalman filter (UKF) is extended to relative attitude estimation and navigation. This approach for nonlinear systems has faster convergence than the approach based on the standard extended Kalman filter (EKF) even with inaccurate initial conditions in attitude estimation and navigation problems. The filter formulation employs measurements obtained from a vision sensor to provide multiple line(-) of(-) sight vectors from the spacecraft to another spacecraft. The line-of-sight measurements are coupled with gyro measurements and dynamic models in an UKF to determine relative attitude, position and gyro biases. A vector of generalized Rodrigues parameters is used to represent the local error-quaternion between two spacecraft. A multiplicative quaternion-error approach is derived from the local error-quaternion, which guarantees the maintenance of quaternion unit constraint in the filter. The scenario for bounded relative motion is selected to verify this extended application of the UKF. Simulation results show that the UKF is more robust than the EKF under realistic initial attitude and navigation error conditions.

Key words: Vision sensor, Unscented Kalman filter, Multiplicative quaternion error, Relative attitude, Relative position

1. Introduction

Formation flying, autonomous rendezvous and proximity operations typically require the high precision determination of relative attitude and position. The vision-based navigation (VISNAV) system can determine these types of information during the terminal phase of a rendezvous (Junkins et al., 1999). The VISNAV system has several advantages such as variable sensor size à different size sensors, wide sensor field of view, rapid image processing, relatively simple electronics, and minimal six-degree of freedom (DOF) data errors (2 mm in position estimates and 0.01o in attitude estimates at rendezvous) (Gunnam et al., 2002). Recently, space missions have relied on global positioning systems (GPS) that are integrated with other sensors including inertial navigation systems (INS), star trackers, and so on. A GPS-only navigation system may not be effective in space missions because it is subject to errors, integrity problems due to multipaths and other sources, or outage due to blockage, atmospheric ionization during re-entry and delta-v maneuvers (Gaylor and Lightsey, 2003). Although an integrated GPS/INS navigation system may meet the navigation requirements of all flight phases of a spacecraft in near-Earth orbit by system complementation, the VISNAV system only can meet the navigation requirement in the terminal phase of rendezvous without any limitations in GPS navigation. The sensor measurements used in this work are based on a VISNAV system which compromises an optical sensor of new kind

combined with the specific flight sources (beacons) to achieve selective or "intelligent vision." The sensor is made of a positioning sensing diode (PSD) placed in the focal plane of a wide angle lens (Junkins et al., 1999; Kim et al., 2007). A PSD-based sensor is mounted on the deputy vehicle, with structured-frequency light emitting diode (LED) beacons mounted on the chief vehicle. When the rectangular silicon of the PSD is illuminated by the energy from the beacon focused by the lens, and this illumination generates electrical currents in four directions. These currents can be processed with appropriate electronic equipment to estimate the energy centroid of an image (Kim et al., 2007). Intelligent vision uses the PSD to see only specific light sources, by modulating the frequency domain of the chief light and applying relatively simple analog signal processing (demodulation). A more detailed description of the VISNAV system can be found in Junkins et al. (1999) and Kim et al. (2007).

The extended Kalman filter (EKF) has been widely used in state estimation. The EKF is based on the approximation of the state distribution as a Gaussian random variable (GRV) which is propagated through first-order linearization of the nonlinear system. The EKF is a suboptimal filter because of the truncation of the higher-order terms to linearize a system. This truncation can cause large errors in the true posterior mean and the covariance of the transformed GRV, which may lead to suboptimal performance of estimation and sometimes divergence of the filter. The EKF may not be able to cope with realistic initial conditions, leading to filter divergence. Alternatives that can avoid the loss of higher-order terms are the unscented Kalman filter (UKF) and the particle filter. In this work, the UKF is applied to state estimation, because of its robustness under realistic initial conditions. The UKF is an extension of the traditional Kalman filter. It estimates nonlinear systems and performs the unscented transformation. The unscented transformation uses set of samples, or sigma points, that are determined from the a priori mean and covariance of the state. The sigma points completely capture the true mean and covariance of the GRV, and when propagates through a nonlinear system, they capture the posterior mean and covariance accurately to the third order of the Taylor series expansion for any nonlinearity (Lefferts et al., 1982). The ability of the UKF to estimate nonlinearities accurately makes it attractive for estimations of spacecraft relative attitudes and navigation, because of course, the state and observation models of spacecraft relative attitude estimation and navigation are inherently nonlinear.

In attitude representation, Euler angles, quaternions, classical Rodrigues parameters (or Gibbs vector), and modified Rodrigues parameters are typically used. Among these parameters, quaternions are attractive because there is no singularity and the kinematic equation is bilinear. As with the EKF, the direct application of the UKF with a quaternion parameterization of attitude yields a non-unit quaternion. The weighted sum of the quaternion samples in the UKF does not produce a unit quaternion space because the UKF is formulated in a vector space and the quaternion samples do not belong to a vector space but lie on a nonlinear manifold. To overcome this shortcoming, a quaternion multiplication, after neglecting higher-order terms in the error quaternion linearization, allows the four-component quaternion to be effectively replaced by a three-component error vector for the predicted covariance computation and quaternion update.

This guarantees that the quaternion unit normalization is maintained in the filter (Cheon and Kim, 2007; Crassidis and Markley, 2003; Shuster, 1993; VanDyke et al., 2006). The vision-based relative spacecraft attitude and position estimation based on the EKF under ideal initial conditions was researched by Kim et al. (2007). For example, Crassidis proposed using the UKF only for spacecraft absolute attitude estimation with realistic initial attitude and gyro bias measurements. Based on this previous research, this paper presents an extension of the UKF formulation to estimate the relative attitude, the relative position, and the relative velocity instead of the absolute attitude estimation only using the VISNAV sensor approach coupled with gyro measurements from each spacecraft. The necessary equations for relative attitude estimation between two spacecraft are derived. The gyro biases of the chief and deputy spacecraft are estimated. Like the standard EKF, the direct use of UKF with a quaternion parameterization of the attitude leads to a non-unit quaternion estimate. To overcome this complication, this study employs an alternative approach that uses a three-component attitude-error vector to present the quaternion error vector (Shuster, 1993). Several three-component representations are possible, including the Gibbs vector, which has a singularity at 180o, and the vector of modified Rodrigues parameters (MRPs), which has a singularity at 360° (Shuster, 1993). Since this approach uses only a three-component representation for the attitude errors, singularity is never encountered in practice. Updates are performed using quaternion multiplication, naturally maintaining the normalization constraint. The error-state vector derived in relative attitude estimation is appended to include information on the relative position and velocity, the radius and the radial rate of the chief, and the true anomaly and its rate. Thus, the objective of this paper is to propose a VISNAV system which estimates the relative attitude, relative position, and relative velocity between the chief and the

deputy spacecraft using the UKF under realistic initial error-conditions.

2. Relative Equations of Motion

This section provides an overview of the model used to describe the relative position and attitude of a bounded out-of-orbit plane formation. From this formation, the relative equations of motion are then derived. Measurement equations are then derived for the VISNAV sensor, providing line-of-sight (LOS) vectors between the chief and the deputy spacecraft. This section presents the relative equations of motion and the methods to establish closed relative orbits. The chief inertial position vector is denoted as $\mathbf{r}_c$, while that of the deputy inertial position vector is expressed as $\mathbf{r}_d$. The relative position vector σ is expressed in Cartesian coordinate components as $\boldsymbol{\gamma}=(x, y, z)^T$. The rotating reference frame used here is the common local-vertical-local horizontal (LVLH) Clohessy-Wiltshire (CW) frame. To derive the relative equations of motion expressed in CW Cartesian coordinates, the deputy position vector is written as $\mathbf{r}_d=\mathbf{r}_c+\boldsymbol{\gamma}$. This geometry is illustrated in Fig. 1.

If the relative orbit coordinates (x, y, z) are small compared to the chief orbit radius $\mathbf{r}_c$, then the equations of motions are given by

$$\ddot{x} - 2\dot{\theta}\left(1+2\frac{r_c}{p}\right) - 2\dot{\theta}\left(\dot{y} - y\frac{\dot{r}_c}{r_c}\right) = 0 \tag{1a}$$

$$\ddot{y} + 2\dot{\theta}\left(\dot{x} - x\frac{\dot{r}_c}{r_c}\right) - y\dot{\theta}^2\left(1-\frac{r_c}{p}\right) = 0 \tag{1b}$$

$$\ddot{z} + \frac{r_c}{p}\dot{\theta}^2 z = 0 \tag{1c}$$

where p is semilatus rectum of the chief, r_c is the chief orbit radius and $\dot{\theta}$ is true anomaly rate of the chief. These
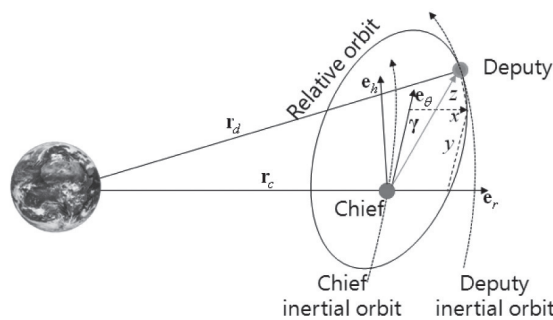

Fig. 1. General type of spacecraft formation with bounded relative motion.

equations of motion are used as the system dynamic model in the filter. The true anomaly acceleration and chief orbit-radius acceleration are given by

$$\ddot{\theta} = -2\frac{\dot{r}_c}{r_c}\dot{\theta} \tag{2a}$$

$$\ddot{r}_c = r_c\dot{\theta}^2\left(1-\frac{r_c}{p}\right) \tag{2b}$$

For generation of bounded relative motion to be used in the simulations, the initial condition at perigee is given by Schaub and Junkins (2003)

$$\frac{\dot{y}_0}{x_0} = \frac{-\tau(2+e)}{\sqrt{(1+e)(1-e)^3}} \tag{3}$$

where τ and e are the mean motion and the eccentricity of the chief, respectively. The equations of motion hereassume that all perturbations are ignored. In reality, of course, there are many perturbations acting on the spacecraft. To validate the estimated states that yield the simulation results discussed below, the relative position and velocity are computed from two orbits expressed in Earth-centered inertial (ECI) reference coordinates and simulated by the high precision orbit propagator (HPOP) of satellite tool kit (STK) (Analytical Graphics Inc.). The true equations of motion, including the perturbations for the chief and deputy, are given by

$$\ddot{\mathbf{r}}_c + \frac{\mu}{r_c^3}\mathbf{r}_c = \sum_i^n \mathbf{F}_i \tag{4a}$$

$$\ddot{\mathbf{r}}_d + \frac{\mu}{r_d^3}\mathbf{r}_d = \sum_i^n \mathbf{F}_i \tag{4b}$$

where μ is the gravitational coefficient and $\sum_i^n \mathrm{F}_i$ the acceleration produced by the perturbations. In the geometry of the chief and deputy spacecrafts with the 3-1-3 rotation sequence illustrated in Fig. 2, the relative position and velocity vectors are derived from the position and velocity vectors using the inertial coordinates of the two spacecrafts. The Euler angles of the rotation sequence are as follows: Ω_c, which is the right ascension of the ascending node, i_c, which is the inclination angle, and θ_c which is the argument of latitude of the chief spacecraft. The position and velocity vectors of the deputy in the inertial coordinate are then expressed as

$$\mathbf{r}_d = \mathbf{r}_c + C^T\boldsymbol{\gamma} \tag{5}$$

$$\mathbf{v}_d = \mathbf{v}_c + C^T\widetilde{\omega}\boldsymbol{\gamma} + C^T\dot{\boldsymbol{\gamma}} \tag{6}$$

26

where C is the 3-1-3 rotation sequence, $C=C_3(u_c)C_1(i_c)$ $C_3(\Omega_c)$, u_c, i_c and Ω_c is the argument of latitude, the inclination and the right ascension of the ascending node of the chaser, respectively. $\dot{\gamma}$ is the relative velocity.

Also,

$$\tilde{\omega} = \begin{bmatrix} 0 & -\dot{\theta} & 0 \\ \dot{\theta} & 0 & 0 \\ 0 & 0 & 0 \end{bmatrix} \tag{7}$$

From Eqs. (5) and (6), the relative position and velocity vectors are determined as

$$\gamma = C(\mathbf{r}_d - \mathbf{r}_c) \tag{8}$$

$$\dot{\gamma} = C(\mathbf{v}_d - \mathbf{v}_c) - \tilde{\omega}\gamma \tag{9}$$

3. Review on Relative Attitude Kinematics, Sensor Models and Unscented Kalman Filtering

This section briefly reviews the attitude kinematic equations using quaternions, the sensor models, and the UKF. In addition, a generalization of the Rodrigues parameter is briefly discussed. The quaternion is defined by $\mathbf{q}=[\mathbf{p}^T \ q^4]^T$, with $\mathbf{p}=[q_1 \ q_2 \ q_3]^T=\hat{\mathbf{e}}\sin(\vartheta/2)$ and $q4=\cos(\vartheta/2)$, where $\hat{\mathbf{e}}$ is the axis of rotation and ϑ is the angle of rotation. Since a four-dimensional vector is used to describe three dimensions, the quaternion components cannot be independent of each other. The quaternion satisfies the normalization constraint $\mathbf{q}^T\mathbf{q}=1$. The (relative) attitude matrix is related to the quaternion by

$$A(\mathbf{q}) = \Xi^T(\mathbf{q})\Psi(\mathbf{q}) \tag{10a}$$

with

$$\Xi(\mathbf{q}) = \begin{bmatrix} q_4 I_{3\times3} + [\mathbf{\rho}\times] \\ -\mathbf{\rho}^T \end{bmatrix} \tag{10b}$$

$$\Psi(\mathbf{q}) = \begin{bmatrix} q_4 I_{3\times3} - [\mathbf{\rho}\times] \\ -\mathbf{\rho}^T \end{bmatrix} \tag{10c}$$

where $I_{3\times3}$ is the 3×3 identity matrix and $[\mathbf{\rho}\times]$ is a cross product matrix since $\mathbf{a}\times\mathbf{b}=[\mathbf{a}\times]\mathbf{b}$, with

$$[\mathbf{a}\times] = \begin{bmatrix} 0 & -a_3 & a_2 \\ a_3 & 0 & -a_1 \\ -a_2 & a_1 & 0 \end{bmatrix} \tag{11}$$

Quaternion multiplication permits successive rotations. Here, the convention of Lefferts et al. (1982) and Shuster (1993) is adopted, in which multiplies what? by the same order as the attitude matrix multiplication, $A(\mathbf{q}')A(\mathbf{q})=A(\mathbf{q}'\otimes\mathbf{q})$. The composition of the quaternion is bilinear, with

$$\mathbf{q}'\otimes\mathbf{q} = \left[\Psi(\mathbf{q}') \ \vdots \ \mathbf{q}'\right]\mathbf{q} = \left[\Xi(\mathbf{q}) \ \vdots \ \mathbf{q}\right]\mathbf{q}' \tag{12}$$

Also, the inverse quaternion is given by $\mathbf{q}^{-1}=[-\mathbf{p}^T \ q_4]$. Note that $\mathbf{q}'\otimes\mathbf{q}^{-1}=[0 \ 0 \ 0 \ 1]^T$, which is the identity quaternion. The quaternion kinematics equation is given by

$$\dot{q} = \frac{1}{2}\Xi(\mathbf{q})\mathbf{\omega} = \frac{1}{2}\Omega(\mathbf{\omega})\mathbf{q} \tag{13a}$$

where

$$\Omega(\mathbf{\omega}) = \begin{bmatrix} -[\mathbf{\omega}\times] & \mathbf{\omega} \\ -\mathbf{\omega}^T & 0 \end{bmatrix} \tag{13b}$$

The local error-quaternion, denoted by $\delta\mathbf{q}=[\delta\mathbf{p}^T \ \delta q_4]$ and defined in the UKF formulation, is represented using a vector of generalized Rodrigues parameters (Crassidis and Markley, 2003; Schaub and Junkins, 1996; Schaub and Junkins, 2003)

$$\delta\mathbf{p} = g\frac{\delta\mathbf{\rho}}{a + \delta q_4} \tag{14}$$

where a is a parameter from 0 to 1, and g is a scale factor. Note when $a = 0$ and $g = 1$, then Eq. (14) gives the Gibbs vector. Furthermore, with $a = g = 1$, then Eq. (15) gives the standard vector of MRPs. The effects of λ and the other parameter a to be explained later are demonstrated by simulations in Crassidis and Markley (2003). For small errors, the attitude portion of the covariance is closely related to the attitude estimation errors for any rotation sequence, given by a simple factor (VanDyke et al., 2006). For example, the Gibbs vector linearizes the half angles. g=2(a+1)is chosen so that $\|\delta\mathbf{p}\|$ is equal to ϑ for small errors. The inverse transformation from $\|\delta\mathbf{p}\|$ to $\delta\mathbf{q}$ is given by[8]

$$\delta q_4 = \frac{-a\|\delta\mathbf{p}\|^2 + g\sqrt{g^2 + (1-a^2)\|\delta\mathbf{p}\|^2}}{g^2 + \|\delta\mathbf{p}\|^2} \tag{15a}$$

$$\delta\mathbf{\rho} = g^{-1}(a + \delta q_4)\delta\mathbf{p} \tag{15b}$$

Vision-based discrete-time attitude measurements for a single sensor are given by Crassidis and Markley (2003), Gunnam et al. (2002), Junkins et al. (1999), and Kim et al. (2007)

$$\tilde{\mathbf{b}}_i = A\mathbf{r}_i + \mathbf{v}_i, \qquad \mathbf{v}_i^T A\mathbf{r}_i = 0 \tag{16}$$

27

where $\widetilde{\mathbf{b}}_i$ denotes the ith observation and the sensor error $\mathbf{v}_i$ is characterized as being approximately Gaussian. This satisfies

$$E\{\mathbf{v}_i\} = 0 \tag{17a}$$

$$E\{\mathbf{v}_i \mathbf{v}_i^T\} = \sigma_i^2 \left[I_{3\times3} - (A\mathbf{r}_i)(A\mathbf{r}_i)^T \right] \tag{17b}$$

where E{ } denotes expectation and $I_{3\times3}$ denotes the 3×3 identity matrix. Multiple (N) vector measurements can be concatenated to form

$$\widetilde{y}_k = \begin{bmatrix} A(\mathbf{q})\mathbf{r}_1 \\ A(\mathbf{q})\mathbf{r}_2 \\ \vdots \\ A(\mathbf{q})\mathbf{r}_N \end{bmatrix} + \begin{bmatrix} \mathbf{v}_1 \\ \mathbf{v}_2 \\ \vdots \\ \mathbf{v}_N \end{bmatrix} \tag{18}$$

The advantage of using the model in Eq. (17b) is that the observation covariance in the UKF formulation can effectively be replaced by a nonsingular matrix given by $\sigma_i^2 I_{3\times3}$ (Schaub and Junkins, 1996; Shuster, 1990; Shuster and Oh, 1981). Hence, the observation covariance matrix used in the UKF from all available LOS vectors is given by

$$R_k = \mathrm{diag}\begin{bmatrix} \sigma_1^2 & \sigma_2^2 & ... & \sigma_N^2 \end{bmatrix} \tag{19}$$

A common sensor that measures the angular rate is a rate-integrating gyroscope. For this sensor, a widely used model is given by Crassidis and Markley (2003) and Kim et al. (2007)

$$\widetilde{\boldsymbol{\omega}} = \boldsymbol{\omega} + \boldsymbol{\beta} + \boldsymbol{\eta}_v \tag{20a}$$

$$\dot{\boldsymbol{\beta}} = \boldsymbol{\eta}_u \tag{20b}$$

where $\widetilde{\boldsymbol{\omega}}$ is the continuous-time measured angular rate, $\boldsymbol{\beta}$ is the drift rate, and $\boldsymbol{\eta}_v$ and $\boldsymbol{\eta}_u$ are independent zero-mean Gaussian white noise processes with

$$E\{\boldsymbol{\eta}_v(t)\boldsymbol{\eta}_v^T(t)\} = I_{3\times3}\,\sigma_v^2\delta(t-\tau) \tag{21a}$$

$$E\{\boldsymbol{\eta}_u(t)\boldsymbol{\eta}_u^T(t)\} = I_{3\times3}\sigma_u^2\delta(t-\tau) \tag{21b}$$

where $\delta(t-\tau)$ is the Dirac delta function. In the standard EKF formulation, given a post-update estimate $\hat{\boldsymbol{\beta}}_k^+$, the post-update angular velocity of the chief or deputy and its propagated gyro bias are

$$\hat{\boldsymbol{\omega}}_k^+ = \widetilde{\boldsymbol{\omega}}_k - \hat{\boldsymbol{\beta}}_k^+ \tag{22a}$$

$$\hat{\boldsymbol{\beta}}_{k+1} = \hat{\boldsymbol{\beta}}_k \tag{22b}$$

Given the post updates $\hat{\boldsymbol{\omega}}_k^+$ and $\hat{\mathbf{q}}_k^+$, the discrete-time

propagation of the relative equation of Eq. (13) is given by Kim et al. (2007)

$$\mathbf{q}_{k+1} = \overline{\Omega}\left(\hat{\boldsymbol{\omega}}_{d_k}\right)\overline{\Gamma}\left(\hat{\boldsymbol{\omega}}_{c_k}\right)\mathbf{q}_k \tag{23}$$

With

$$\overline{\Omega}\left(\boldsymbol{\omega}_{d_k}\right) = \begin{bmatrix} \cos\left(\frac{1}{2}\|\boldsymbol{\omega}_{d_k}\|\Delta t\right)I_{3\times3} - [\psi_k \times] & \psi_k \\ -\psi_k^T & \cos\left(\frac{1}{2}\|\boldsymbol{\omega}_{d_k}\|\Delta t\right) \end{bmatrix} \tag{24a}$$

$$\overline{\Gamma}\left(\boldsymbol{\omega}_{c_k}\right) = \begin{bmatrix} \cos\left(\frac{1}{2}\|\boldsymbol{\omega}_{c_k}\|\Delta t\right)I_{3\times3} - [\zeta_k \times] & -\zeta_k \\ -\zeta_k^T & \cos\left(\frac{1}{2}\|\boldsymbol{\omega}_{c_k}\|\Delta t\right) \end{bmatrix} \tag{24b}$$

where

$$\psi_k = \frac{\sin\left(\frac{1}{2}\|\boldsymbol{\omega}_{d_k}\|\Delta t\right)\boldsymbol{\omega}_{d_k}}{\|\boldsymbol{\omega}_{d_k}\|} \tag{25a}$$

$$\zeta_k = \frac{\sin\left(\frac{1}{2}\|\boldsymbol{\omega}_{c_k}\|\Delta t\right)\boldsymbol{\omega}_{c_k}}{\|\boldsymbol{\omega}_{c_k}\|} \tag{25b}$$

and Δt is the sampling interval. Note that the matrices $\overline{\Omega}(\boldsymbol{\omega}_{d_c})$ and $\overline{\Gamma}(\boldsymbol{\omega}_{c_c})$ also commute. In this section, the UKF is also reviewed. Many difficulties in the EKF arise arises because of its linearization of a nonlinear system. To overcome the disadvantages of the EKF, the UKF uses an unscented transformation. Unlike the EKF, the UKF does not require Jacobian and Hessian computations. Rather, the UKF uses a minimal set of sigma points, deterministically chosen from the error covariance and propagated through the true nonlinear system to capture the posterior mean and covariance of the Gaussian random variable accurately for the third order Taylor series expansion for any nonlinearity (Cheng et al., 2006; Julier and Uhlmann, 2004; Wan and Van Der Merwe, 2000). (…to capture …covariance …accurately for the …)Consider the system model of discrete-time nonlinear equations

$$\mathbf{x}_{k+1} = \mathbf{f}(x_k, k) + G_k\mathbf{w}_k \tag{26a}$$

$$\mathbf{y}_k = \mathbf{h}_k(\mathbf{x}_k, k) + \mathbf{v}_k \tag{26b}$$

where $\mathbf{x}_k$ is the $n\times1$ state vector and $\mathbf{y}_k$ is the $m\times1$ observation vector. Note, that a continuous time model can always be expressed in the form of Eq. (26a) through an appropriate

28

numerical integration scheme.7 The process noise vector $\mathbf{w}_k$ and observation noise vector $\mathbf{v}_k$ are assumed to be zero-mean and white Gaussian noise, and the covariances of these vectors are given by Q_k and R_k, respectively. From the $n \times n$ covariance P_k, a set of $(2n+1)$ sigma points $\mathbf{X}_k \in^{2n+1}$ can be generated by the columns of the matrices $\sqrt{(n+\lambda)P_k}$. The general formulation for the propagation equations begins with a set of sigma points with corresponding weights W_i, according to the following:

$$\boldsymbol{\chi}_k(0) = \hat{\mathbf{x}}_k \tag{27a}$$

$$\boldsymbol{\chi}_k(i) = \hat{\mathbf{x}}_k + \left(\gamma \sqrt{\left(P_k + \overline{Q}_k\right)} \right)_i \quad for\ i = 1,\ldots,n \tag{27b}$$

$$\boldsymbol{\chi}_k(i) = \hat{\mathbf{x}}_k - \left(\gamma \sqrt{\left(P_k + \overline{Q}_k\right)} \right)_i \quad for\ i = n+1,\ldots,2n$$

$$(27c)\ W_0 = \frac{\lambda}{(n+\lambda)} \tag{28a}$$

$$W_i = \frac{1}{\{2(n+\lambda)\}} \qquad i = 1,\ldots 2n \tag{28b}$$

where the matrix $\overline{Q}_k$ for attitude estimation is related only to the process noise covariance for Eq. (26a). However, Q_k is not the corresponding covariance due to the second term in Eq. (26a). Note $\gamma = \sqrt{(n+\lambda)}$ and λ are convenient parameters in taking advantage of whatever knowledge is available of the higher moments of the given distribution. In scalar systems, where n = 1, a value of $\lambda = 2$ leads to sixth order errors in the mean and variance that are of sixth order. For higher dimensional systems, choosing $\lambda = 3 - n$ minimizes the mean-squared-error up to the fourth order (Banani and Masnadi-Shirazi, 2007; Cheon and Kim, 2007). However, caution is required when λ is negative since the predicted covariance may become a positive semi-definite covariance matrix. Also, when $n+\lambda$ tends to zero, the mean tends to be that calculated by the truncated second-order filter. The matrix square root $\sqrt{(P_k+\overline{Q}_k)}$ can be calculated by a lower triangular Cholesky factorization (Julier et al., 1995). From Eq. (27), the matrix $\boldsymbol{\chi}_k$ of $2n+1$ sigma vectors $\boldsymbol{\chi}_{i,k}$ is formed as

$$\boldsymbol{\chi}_k = \left[\hat{\mathbf{x}}_k \quad \hat{\mathbf{x}}_k + \gamma \sqrt{\left(P_k + \overline{Q}_k\right)} \quad \hat{\mathbf{x}}_k - \gamma \sqrt{\left(P_k + \overline{Q}_k\right)} \right] \tag{29}$$

The transformed set of sigma points is evaluated for each of the points by

$$\boldsymbol{\chi}_{k+1}(i) = \mathbf{f}\big(\chi_k(i), k\big) \tag{30}$$

where $\chi_{k+1}(i)$ is the ith column of χ_k. The predicted mean

$\hat{\mathbf{x}}_{k+1}^-$ and the predicted covariance $\boldsymbol{P}_{k+1}^-$ are computed using a weighted sample mean and the covariance of the posterior sigma point vectors as

$$\mathbf{x}_{k+1}^-(i) = \sum_{i=0}^{2n} W_i\, \boldsymbol{\chi}_{k+1}(i) \tag{31}$$

$$\mathrm{P}_{k+1}^- = \sum_{i=0}^{2n} W_i \left\{ \boldsymbol{\chi}_{k+1}(i) - \mathbf{x}_{k+1}^-(i) \right\} \left\{ \boldsymbol{\chi}_{k+1}(i) - \mathbf{x}_{k+1}^-(i) \right\}^T + \overline{Q}_k \tag{32}$$

The mean observation is given by

$$\hat{\mathbf{y}}_{k+1}^- = \sum_{i=0}^{2n} W_i\, \mathbf{Y}_{k+1}(i) \tag{33}$$

$$\mathbf{Y}_{k+1}(i) = \mathbf{h}\big(\boldsymbol{\chi}_{k+1}(i), k+1\big) \tag{34}$$

The predicted output covariance P_{k+1}^{yy} is given by

$$\mathrm{P}_{k+1}^{yy} = \sum_{i=0}^{2n} W_i \left\{ \mathbf{Y}_{k+1}(i) - \hat{\mathbf{y}}_{k+1}^-(i) \right\} \left\{ \mathbf{Y}_{k+1}(i) - \hat{\mathbf{y}}_{k+1}^-(i) \right\}^T \tag{35}$$

The innovation covariance P_{k+r}^{vv} is then computed by

$$P_{k+1}^{vv} = P_{k+1}^{yy} + R_{k+1} \tag{36}$$

The filter gain K_{k+1} is computed by

$$K_{k+1} = P_{k+1}^{xy} \left(P_{k+1}^{vv}\right)^{-1} \tag{37}$$

and the cross correlation matrix is given by

$$\mathbf{P}_{k+1}^{xy} = \sum_{i=0}^{2n} W_i \left\{ \boldsymbol{\chi}_{k+1}(i) - \mathbf{y}_{k+1}(i) \right\} \left\{ \boldsymbol{\chi}_{k+1}(i) - \mathbf{y}_{k+1}(i) \right\}^T \tag{38}$$

The estimated state vector $\hat{\mathbf{x}}_{k+1}^+$ and updated covariance P_{k+1}^+ are given by

$$\hat{\mathbf{x}}_{k+1}^+ = \hat{\mathbf{x}}_{k+1}^+ + K_{k+1}\left(y_{k+1} - \hat{\mathbf{y}}_{k+1}^-\right) \tag{39}$$

$$P_{k+1}^+ = P_{k+1}^- - K_{k+1} P_{k+1}^{vv} K_{k+1}^T \tag{40}$$

4. Unscented Relative Attitude Filter

This section shows the derivation of the UKF for relative attitude estimation. In general, the UKF cannot be implemented directly with the equations in Section III because of the violation of the unit quaternion constraint. It is difficult to compute the means of a set of sigma points because the rotation represented by the quaternion does not belong to a vector space, but lies on a nonlinear manifold. Furthermore, the quaternion is constrained to the three-dimensional

unit sphere of a four-dimensional Euclidian space. The quaternion predicted mean using Eq. (31) is not guaranteed to maintain a unit quaternion because the quaternion is not mathematically closed for addition and scalar multiplication. This limitation makes the straightforward implementation of the UKF with quaternions undesirable. On the other hand, an EKF can be designed using this approach, in which the quaternion normalization is performed by "brute force." To use the UKF, an unconstrained three component vector is used to represent the attitude error quaternion. First, the state vector is defined as

$$\boldsymbol{\chi}_k(0) = \hat{\mathbf{x}}_k = \begin{bmatrix} \delta\hat{\mathbf{p}}_k^+ \\ \hat{\boldsymbol{\beta}}_{c_k}^+ \\ \hat{\boldsymbol{\beta}}_{d_k}^+ \end{bmatrix} \tag{41}$$

where $\delta\hat{\mathbf{p}}_k^+$ is the updated vector of generalized Rodrigues parameters, and $\hat{\boldsymbol{\beta}}_{ck}^+$ and $\hat{\boldsymbol{\beta}}_{dk}^+$ are the updated gyro bias of the chief and the deputy spacecraft, respectively. Using $\delta\hat{\mathbf{p}}_k^+$ from Eq. (14), the nominal quaternion is propagated and updated. The overall covariance is a 9×9 matrix, and this three-dimensional representation is unconstrained. The use of Eq. (31) causes no difficulty, providing an attractive method of attitude representation. First, the vector $\boldsymbol{\chi}_k(i)$ in Eq. (27) is partitioned into

$$\boldsymbol{\chi}_k(i) = \begin{bmatrix} \boldsymbol{\chi}_k^{\delta p}(i) \\ \boldsymbol{\chi}_k^{\beta_c}(i) \\ \boldsymbol{\chi}_k^{\beta_d}(i) \end{bmatrix}, \ i = 0, 1, \ldots, 18 \tag{42}$$

where $\boldsymbol{\chi}_k^{\delta p}$ is the attitude-error, $\boldsymbol{\chi}_k^{\beta_c}(i)$ is the chief gyro bias and $\boldsymbol{\chi}_k^{\beta_d}(i)$ is the deputy gyro bias. Since the unit quaternion is not closed for addition and subtraction, the transformed sigma points of the quaternion are not simply constructed, while the sigma points for the gyro bias are calculated by Eq. (27). Rather, the transformed sigma points of the quaternion are also quaternions satisfying the normalization constraints and should be scattered around the current quaternion estimate on the unit sphere. Therefore, the transformed quaternion sigma points are generated by multiplying the error quaternion by the current estimate. To generate quaternion samples evenly on the unit sphere around the current quaternion estimate, both the error quaternion and the inverse of the quaternion $\delta\mathbf{q}_{i,k}^+$ and $(\delta\mathbf{q}_{i,k}^+)^{-1}$ are used. The sigma point quaternions are then computed using

$$\boldsymbol{\chi}_{0,k}^q = \hat{\mathbf{q}}_k^+ \tag{43a}$$

$$\boldsymbol{\chi}_{i,k}^q = \delta\hat{\mathbf{q}}_{i,k}^+ \otimes \hat{\mathbf{q}}_k^+ \quad \text{for } i = 1,\ldots, 9 \tag{43b}$$

$$\boldsymbol{\chi}_{0,k}^q = \left(\delta\hat{\mathbf{q}}_k^+\right)^{-1} \otimes \hat{\mathbf{q}}_{i,k}^+ \quad \text{for } i = 10,\ldots, 18 \tag{43c}$$

where $\delta\mathbf{q}_k^+(i) = [\delta\boldsymbol{\rho}_k^{+T} \ \delta\mathbf{q}_{4,k}^+(i)]^T$ is represented by Eq. (15) as

$$\delta q_{4,k}^+(i) = \frac{-a\left\|\boldsymbol{\chi}_k^{\delta p}(i)\right\|^2 + g\sqrt{g^2 + \left(1 - a^2\right)\left\|\boldsymbol{\chi}_k^{\delta p}(i)\right\|^2}}{g^2 + \left\|\boldsymbol{\chi}_k^{\delta p}(i)\right\|^2} \quad \text{for } i$$

$$= 1, 2, \ldots, 18 \tag{44a}$$

$$\delta\mathbf{p}_k^+(i) = g^{-1}\left[a + \delta q_{4,k}^+(i)\right]\boldsymbol{\chi}_k^{\delta p}(i) \quad \text{for } i = 1,2, \ldots, 18 \tag{44b}$$

Eq. (40a) clearly requires that $\boldsymbol{\chi}_k^{\delta p}(0)$ be zero since the attitude error is reset to zero after the update, and this resetting moves information from one part of the estimate to another part. For the definition of sigma points, the gyro bias part of the chief and the deputy from $\gamma\sqrt{P_k + \overline{Q}_k}$ in Eq. (29) are denoted as $\boldsymbol{\zeta}_k^{\beta_c}$ and $\boldsymbol{\zeta}_k^{\beta_d}$, respectively. The sigma points corresponding to the quaternion actually depend on the quaternion itself, regardless of the chief and the deputy bias. All sigma points are constructed as

$$\boldsymbol{\chi}_k(i) = \begin{bmatrix} \boldsymbol{\chi}_k^{\delta p}(i) \\ \boldsymbol{\chi}_k^{\beta_c}(i) \\ \boldsymbol{\chi}_k^{\beta_d}(i) \end{bmatrix} = \begin{bmatrix} \hat{\mathbf{q}}_k^+ & \delta\hat{\mathbf{q}}_k^+ \oplus \hat{\mathbf{q}}_k^+ & \left(\delta\hat{\mathbf{q}}_k^+\right)^{-1} \oplus \hat{\mathbf{q}}_k^+ \\ \hat{\boldsymbol{\beta}}_{c_k}^+ & \hat{\boldsymbol{\beta}}_k^+ + \boldsymbol{\zeta}_k^{\beta_c} & \hat{\boldsymbol{\beta}}_k^+ - \boldsymbol{\zeta}_k^{\beta_c} \\ \hat{\boldsymbol{\beta}}_{d_k}^+ & \hat{\boldsymbol{\beta}}_k^+ + \boldsymbol{\zeta}_k^{\beta_d} & \hat{\boldsymbol{\beta}}_k^+ - \boldsymbol{\zeta}_k^{\beta_d} \end{bmatrix} \tag{45}$$

Now these transformed quaternions are propagated forward to k+1 by Eq. (46) as

$$\mathbf{q}_{k+1}(i) = \overline{\Omega}\left(\hat{\boldsymbol{\omega}}_{d_k}\right)\overline{\Gamma}\left(\hat{\boldsymbol{\omega}}_{c_k}\right)\mathbf{q}_k(i) \quad i = 0, 1, \ldots, 18 \tag{46}$$

where the estimated angular velocities of the chief and the deputy are given by Eq. (47) as

$$\hat{\boldsymbol{\omega}}_{c_k}^+(i) = \widetilde{\boldsymbol{\omega}}_{c_k}(i) - \boldsymbol{\chi}_k^{\beta_c}(i) \quad i = 0, 1, \ldots, 18 \tag{47a}$$

$$\hat{\boldsymbol{\omega}}_{d_k}^+(i) = \widetilde{\boldsymbol{\omega}}_{d_k}(i) - \boldsymbol{\chi}_k^{\beta_d}(i) \quad i = 0, 1, \ldots, 18 \tag{47b}$$

Note that $\boldsymbol{\chi}_k^{\beta_c}(0)$ is the zeroth-bias sigma point given by the current estimate $\boldsymbol{\chi}_k^{\beta_c}(0) = \hat{\boldsymbol{\beta}}_{c}^+$, $\boldsymbol{\chi}_k^{\beta_d}(0) = \hat{\boldsymbol{\beta}}_{d}^+$. The propagated quaternion is computed using

$$\delta\hat{\mathbf{q}}_{i,k}^- = \delta\hat{\mathbf{q}}_{i,k}^- \otimes \left[\hat{\mathbf{q}}_k^-(0)\right]^{-1} \quad , i = 0, 1, \ldots, 18 \tag{48}$$

Note that $\hat{\mathbf{q}}_k^-(0)$ is the identity quaternion. Finally, the propagated sigma points can be computed using the representation of Eq. (14) as

$$\boldsymbol{\chi}_{k+1}^{\delta p}(0) = \mathbf{0}_{3\times1} \tag{49a}$$

$$\boldsymbol{\chi}_{k+1}^{\delta p}(i) = g\frac{\delta\mathbf{p}_{k+1}^-(i)}{a + \delta q_{4_{k+1}}^-(i)}, i = 0, 1, \ldots, 18 \tag{49b}$$

30

with $[\delta\boldsymbol{\rho}_{k+1}^{-T}(i) \quad \delta q_{4k+1}^{-}(i)]^T = \delta\mathbf{q}_{k+1}^{-T}(i)$. Furthermore, from Eq. (22b)

$$\boldsymbol{\chi}_{k+1}^{\beta_c}(i) = \boldsymbol{\chi}_k^{\beta_c}(i), \quad i = 0, 1, \ldots, 18 \tag{50a}$$

$$\boldsymbol{\chi}_{k+1}^{\beta_d}(i) = \boldsymbol{\chi}_k^{\beta_d}(i), \quad i = 0, 1, \ldots, 18 \tag{50b}$$

The predicted mean and covariance can now be computed using Eqs. (31) and (32), respectively. The output covariance, innovation covariance, and cross-correlation matrices are computed using Eqs. (35), (36), and (38), respectively. Next, the state vector and covariance are updated using Eqs. (39) and (40) with $\hat{\mathbf{x}}_{k+1}^{-} = [\delta\hat{\mathbf{p}}_k^{+T} \quad \hat{\boldsymbol{\beta}}_{c_k}^{+T} \quad \hat{\boldsymbol{\beta}}_{d_k}^{+T}]^T$. The quaternion is then updated using

$$\hat{\mathbf{q}}_{k+1}^{+} = \delta\hat{\mathbf{q}}_{k+1}^{+} \otimes \hat{\mathbf{q}}_{k+1}^{-}(0) \tag{51}$$

Note that $\delta q_{k+1}^{+} = [\delta\boldsymbol{\rho}_{k+1}^{+T} \quad \delta q_{4k+1}^{+}]^T$ is represented by Eq. (15) as

$$\delta q_{4_{k+1}}^{+} = \frac{-\mathrm{a}\left\|\delta\hat{\mathbf{p}}_{k+1}^{+}\right\|^2 + \mathrm{g}\sqrt{\mathrm{g}^2 + \left(1 - \mathrm{a}^2\right)\left\|\delta\hat{\mathbf{p}}_{k+1}^{+}\right\|^2}}{\mathrm{g}^2 + \left\|\delta\hat{\mathbf{p}}_{k+1}^{+}\right\|^2} \tag{52a}$$

$$\delta\boldsymbol{\rho}_{k+1}^{+} = \mathrm{g}^{-1}\left(\mathrm{a} + \delta q_{4_{k+1}}^{+}\right)\delta\mathbf{p} \tag{52b}$$

Finally, $\delta\hat{\mathbf{p}}_{k+1}^{+}$ is reset to zero for the next propagation.

5. Relative Attitude, Position and Velocity Estimation

This section shows the derivation of the necessary equations for both relative attitude estimation and relative navigation, accounting for relative position and velocity. The state vector in the attitude-only formulations shown in the previous section is now appended to include the relative position and velocity of the deputy, the radius and radial rate of the chief spacecraft and the true anomaly and its rate. This appended vector is given by Kim et al. (2007)

$$\begin{aligned}
\mathbf{X} &= \begin{bmatrix} x & y & z & \dot{x} & \dot{y} & \dot{z} & r_c & \dot{r}_c & \theta & \dot{\theta} \end{bmatrix}^T \\
&= \begin{bmatrix} x_1 & x_2 & x_3 & x_4 & x_5 & x_6 & x_7 & x_8 & x_9 & x_{10} \end{bmatrix}^T
\end{aligned} \tag{53}$$

The nonlinear state-space model follows Eqs. (1) and (2) as

$$\dot{\mathbf{X}} = \mathbf{f}(\mathbf{X}) = \begin{bmatrix} x_4 \\ x_5 \\ x_6 \\ x_1 x_{10}^2\left(1 + 2x_7/p\right) + 2x_{10}\left(x_5 - x_2 x_8/x_7\right) \\ -2x_{10}\left(x_4 - x_1 x_8/x_7\right) + x_2 x_{10}^2\left(1 - x_7/p\right) \\ -x_7 x_{10}^2 x_3/p \\ x_8 \\ x_7 x_{10}^2\left(1 - x_7/p\right) \\ x_{10} \\ -2x_8 x_{10}/x_7 \end{bmatrix} \tag{54}$$

In this formulation, the chief radius and true anomaly are estimated, along with their respective derivatives. If this information is assumed to be known initially, then these states can be removed and their observed values can be added as process noise in the state model. The necessary equations for relative attitude estimation between two spacecraft are derived in Kim et al. (2007). Among the three ways to represent the state presented in Kim et al. (2007) based on the EKF, this work selected the estimation of relative attitude and individual gyro biases for the chief and the deputy spacecraft. From the derived error-state dynamics, the discrete-time covariance matrix is computed and is applied equally to the UKF. The linearization process makes the following assumptions, which are valid to within first-order (Lefferts et al., 1982):

$$\delta\mathbf{q} = \begin{bmatrix} \frac{1}{2}\delta\boldsymbol{\alpha} \\ 1 \end{bmatrix} \tag{55a}$$

$$\mathrm{A}(\mathbf{q}) = \left\{\mathbf{I}_{3\times 3} - [\delta\boldsymbol{\alpha}\times]\right\}\mathrm{A}(\hat{\mathbf{q}}) \tag{55b}$$

where $\delta\boldsymbol{\alpha}$ is a small angle-error correction. Then, the error-state dynamics for the relative attitude estimation is given by Kim et al. (2007)

$$\Delta\dot{\mathbf{x}} = F\Delta\mathbf{x} + G\mathbf{w} \tag{56}$$

with

$$\Delta\mathbf{x} = \begin{bmatrix} \delta\boldsymbol{\alpha}^T & \delta\boldsymbol{\beta}_c^T & \delta\boldsymbol{\beta}_d^T \end{bmatrix}^T \tag{57a}$$

$$\mathbf{w} = \begin{bmatrix} \boldsymbol{\eta}_{cv}^T & \boldsymbol{\eta}_{dv}^T & \boldsymbol{\eta}_{cu}^T & \boldsymbol{\eta}_{du}^T \end{bmatrix}^T \tag{57b}$$

where

$$F = \begin{bmatrix} -[\omega_d\times] & \mathrm{A}(\hat{\mathbf{q}}) & -I_{3\times 3} \\ 0_{3\times 3} & 0_{3\times 3} & 0_{3\times 3} \\ 0_{3\times 3} & 0_{3\times 3} & 0_{3\times 3} \end{bmatrix} \tag{58a}$$

$$G = \begin{bmatrix} A(\hat{q}) & -I_{3\times3} & 0_{3\times3} & 0_{3\times3} \\ 0_{3\times3} & 0_{3\times3} & I_{3\times3} & 0_{3\times3} \\ 0_{3\times3} & 0_{3\times3} & 0_{3\times3} & I_{3\times3} \end{bmatrix} \qquad (58b)$$

and the spectral density matrix of the process noise **w** is given by

$$Q = \begin{bmatrix} \sigma_{cv}^2 I_{3\times3} & 0_{3\times3} & 0_{3\times3} & 0_{3\times3} \\ 0_{3\times3} & \sigma_{dv}^2 I_{3\times3} & 0_{3\times3} & 0_{3\times3} \\ 0_{3\times3} & 0_{3\times3} & \sigma_{cu}^2 I_{3\times3} & 0_{3\times3} \\ 0_{3\times3} & 0_{3\times3} & 0_{3\times3} & \sigma_{du}^2 I_{3\times3} \end{bmatrix} \qquad (59)$$

For the estimation of relative attitude and the states in Eq. (53) together, the error-state vector for the chief and deputy gyro bias case is now a combination of Eqs. (53) and (57a) as

$$\Delta\mathbf{x} = \begin{bmatrix} \delta\boldsymbol{\alpha}^T \ \Delta\boldsymbol{\beta}_c^T \ \Delta\boldsymbol{\beta}_d^T \ \Delta\boldsymbol{\gamma}^T \ \Delta\dot{\boldsymbol{\gamma}}^T \ \Delta r_c \ \Delta\dot{r}_c \ \Delta\theta \ \Delta\dot{\theta} \end{bmatrix}_{19\times1} \qquad (60)$$

with the obvious definitions of $\Delta\boldsymbol{\gamma}$, $\Delta\dot{\boldsymbol{\gamma}}$, Δr, $\Delta\dot{r}_c$, $\Delta\theta$ and $\Delta\dot{\theta}$. The matrices F and G used in the EKF covariance propagation are also used for the UKF sigma point generation in Eq. (27) and for the predicted output covariance Eq. (35). These augmented matrices are given by

$$F_{aug} = \begin{bmatrix} -[\hat{\omega}_d\times] & A(\hat{\mathbf{q}}) & -I_{3\times3} & 0_{3\times3} \\ 0_{3\times3} & 0_{3\times3} & 0_{3\times3} & 0_{3\times3} \\ 0_{3\times3} & 0_{3\times3} & 0_{3\times3} & 0_{3\times3} \\ 0_{3\times3} & 0_{3\times3} & 0_{3\times3} & \left.\dfrac{\partial\mathbf{f}(\mathbf{X})}{\partial\mathbf{X}}\right|_{\hat{\mathbf{X}}} \end{bmatrix}_{19\times19} \qquad (61)$$

where $\hat{\mathbf{X}}$ denotes the estimate of **X**. The partial derivative $\partial\mathbf{f(X)}/\partial\mathbf{X}$ is straightforward, but for brevity, is not shown here. The augmented matrix G_{aug} is given by

$$G_{aug} = \begin{bmatrix} A(\hat{\mathbf{q}}) & -I_{3\times3} & 0_{3\times3} & 0_{3\times3} & 0_{3\times3} \\ 0_{3\times3} & 0_{3\times3} & I_{3\times3} & 0_{3\times3} & 0_{3\times3} \\ 0_{3\times3} & 0_{3\times3} & 0_{3\times3} & I_{3\times3} & 0_{3\times3} \\ 0_{3\times3} & 0_{3\times3} & 0_{3\times3} & 0_{3\times3} & I_{3\times3} \\ 0_{3\times3} & 0_{3\times3} & 0_{3\times3} & 0_{3\times3} & 0_{3\times3} \\ 0_{2\times3} & 0_{2\times3} & 0_{2\times3} & 0_{2\times3} & 0_{2\times3} \\ 0_{2\times3} & 0_{2\times3} & 0_{2\times3} & 0_{2\times3} & 0_{2\times3} \end{bmatrix} \qquad (62)$$

Defining the new process noise vector as $\boldsymbol{w}=[\boldsymbol{\eta}_{cv}^T \ \boldsymbol{\eta}_{dv}^T \ \boldsymbol{\eta}_{cu}^T \ \boldsymbol{\eta}_{dv}^T \ w_x \ w_y \ w_z]_{15\times1}^T$, the new augmented matrix Q_{aug} is given by

$$Q_{aug} = \begin{bmatrix} \sigma_{cv}^2 I_{3\times3} & 0_{3\times3} & 0_{3\times3} & 0_{3\times3} & 0_{3\times1} & 0_{3\times1} & 0_{3\times1} \\ 0_{3\times3} & \sigma_{dv}^2 I_{3\times3} & 0_{3\times3} & 0_{3\times3} & 0_{3\times1} & 0_{3\times1} & 0_{3\times1} \\ 0_{3\times3} & 0_{3\times3} & \sigma_{cu}^2 I_{3\times3} & 0_{3\times3} & 0_{3\times1} & 0_{3\times1} & 0_{3\times1} \\ 0_{3\times3} & 0_{3\times3} & 0_{3\times3} & \sigma_{du}^2 I_{3\times3} & 0_{3\times1} & 0_{3\times1} & 0_{3\times1} \\ 0_{1\times3} & 0_{1\times3} & 0_{1\times3} & 0_{1\times3} & w_x^2 & 0 & 0 \\ 0_{1\times3} & 0_{1\times3} & 0_{1\times3} & 0_{1\times3} & 0 & w_y^2 & 0 \\ 0_{1\times3} & 0_{1\times3} & 0_{1\times3} & 0_{1\times3} & 0 & 0 & w_z^2 \end{bmatrix} \qquad (63)$$

Solutions for the state transition matrix F in Eq. (56) and the discrete-time process noise covariance are intractable due to the dependence of both on the attitude matrix (Kim et al., 2007). For the convergence of the state, w_x, w_y, w_z in Eq. (63) should be properly tuned experimentally, considering the scale of the relative disturbances that exist in HPOP modeling. A numerical solution is given by van Loan for fixed parameter systems, which includes a constant sampling interval, the time invariant state, and covariance matrices (Brown and Hwang, 1997; Van Loan, 1978). First, a 38×38 matrix, $\bar{A}$, is formed as

$$\bar{A} = \begin{bmatrix} -F_{aug} & G_{aug}Q_{aug}G_{aug}^T \\ 0_{19\times19} & F_{aug}^T \end{bmatrix}\Delta t \qquad (64)$$

Then, the matrix exponential of Eq. (64) is computed as

$$\bar{B} = e^{\bar{A}} = \begin{bmatrix} \bar{B}_{11} & \bar{B}_{12} \\ 0_{19\times19} & \bar{B}_{22} \end{bmatrix} = \begin{bmatrix} \bar{B}_{11} & \Phi^{-1}\bar{B}_{12} \\ 0_{19\times19} & \Phi^T \end{bmatrix} \qquad (65)$$

where Φ is the state transition matrix of F in Eq. (56) and $\bar{Q}_{aug}$ is the augmented discrete-time covariance matrix. The state transition matrix and discrete-time process noise covariance are then given by

$$\Phi^{-1} = B_{22}^T \qquad (66a)$$

$$\bar{Q}_{aug} = \Phi B_{12} \qquad (66b)$$

6. Simulation Results

6.1 Bounded relative motion

In this section, the performances between UKF and EKF approaches are compared several times through simulated examples using STK for realistic relative navigation between the International Space Station (ISS), which is the chief, and the Space Shuttle, which is the deputy. For this simulation, a bounded relative motion constraint is applied using Eq. (3). The ground tracks and orbits of the two spacecrafts appear almost identical. The scenario begins at the perigee

of the chief and proceeds over ten hours of bounded relative motion. The initial condition for the vector X in appropriate units of meters, meters per second, radians and radians per second is given by

$$\mathbf{X}(t_0)=[200\ 200\ 100\ 0.01\ -0.45723\ 0.01$$
$$6.73173488\times10^6\ 0\ 0\ 0.0011437] \quad (67)$$

The simulation time for the relative motion between the two spacecrafts is 600 minutes, and step size is 10 seconds. The orbit period of the chief is nearly 92 minutes. For the entire simulation, the true relative attitude is simulated by propagating Eq. (23) using an initial quaternion given by $\mathbf{q}(t_0)=[\sqrt{2}/2\ \ 0\ \ 0\ \ \sqrt{2}/2]^T$ and angular velocities given by $\boldsymbol{\omega}_c=[0\ \ 0.0011\ \ -0.0011]$ rad/sec and $\boldsymbol{\omega}_d=[-0.002\ \ 0\ \ 0.0011]$ rad/sec. The gyro noise parameters are given by $\sigma_{cu}=\sigma_{du}=\sqrt{10}\times10^{-10}$ rad/sec3/2 and $\sigma_{cv}=\sigma_{dv}=\sqrt{10}\times10^{-5}$ rad/sec$^{1/2}$ (Kim et al., 2007). The initial biases for each axis of both the chief and the deputy gyros are given as 1 deg/hr. Six beacons are assumed to exist on the chief, and their configuration is shown in Fig. 2. These beacons are assumed to be visible to the PSD on the deputy throughout the entire simulation run. Simulated VISNAV measurements are generated using Eq. (16) with a standard observation deviation of 0.0005 degrees. Each covariance sub-matrix for attitude, gyro biases, position and velocity is assumed to be isotropic, a diagonal matrix with equal elements.

To validate the estimated relative position and velocity, a simulation truth model is generated with Eq. (1) by adding acceleration disturbances to the right side, which are modeled as zero-mean Gaussian white-noise process (Kim et al., 2007). However, this model may not be sufficiently realistic. To address this issue, a high-fidelity propagator may be used instead to generate "true" spacecraft ephemerides. For a more realistic validation, both spacecrafts are modeled with HPOP of STK (Analytical Graphics Inc.) using the force model in Table 1. The simulated truth model is computed using Eqs. (5-9).
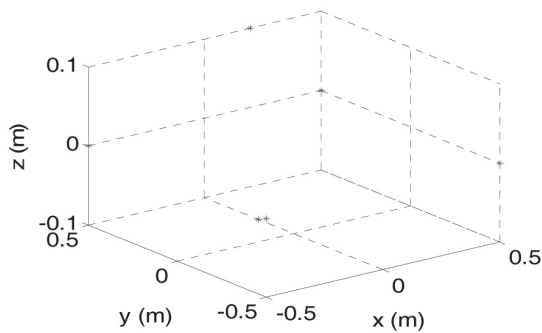

Fig. 2. Beacons configuration in Clohessy-Wiltshire frame[4].

Table 1. Inertial propagation force model

High precision orbit propagator
Gravity field degree and order (70 × 70)
Atmospheric drag
Solar radiation drag
Third body gravity (Moon and Sun)

The first simulations with both the UKF and the EKF are performed under ideal conditions, i.e. with no initial attitude errors, initial bias estimates set to zero, and no initial position and velocity errors. The initial attitude covariance is set to $P_{att}=I_{3\times3}(deg)^2$, and the initial chief and deputy gyro bias covariances are each set to ??. $P_{bias}=4I_{3\times3}(deg/hr)^2$, the initial position covariance is set to $P_{pos}=5I_{3\times3}$m^2 and the initial velocity covariance is set to $P_{vel}=0.02I_{3\times3}$(m/s)^2. The initial variance for the chief position is set to 1,000 m^2 and the velocity variance is set to 0.01 (m/s)^2. The initial variance for the true anomaly is set to 1×10^{-4} (rad)^2, and the rate variance is set to 1×10^{-4} (rad/sec)^2. The gyro and LOS are both sampled at 10 seconds intervals for 600 minutes. Also, $a=1$ with $g=4$, which gives four times the vector of MRPs for the error representation, and $\lambda=1$ is chosen for these simulations. Figure 3 shows the
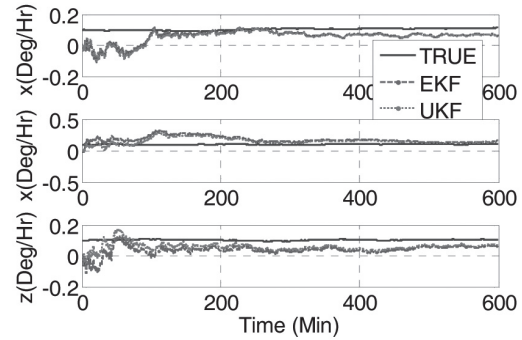

(a) Chief bias estimate
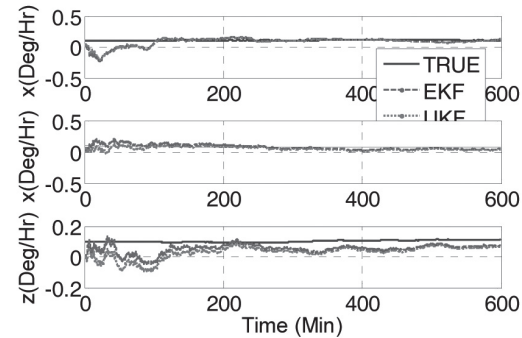
(b) Deputy bias estimate

Fig. 3. Gyro bias estimate.

accurate estimation of the chief and deputy biases. Figure 4 shows the attitude errors and respective 3σ bounds derived from the UKF and the EKF.

Figure 5 shows that the norm of the attitude errors is less than 10⁻¹ deg. Figure 6, the estimated relative orbit, shows that the error is bounded by less than ±0.5 m in three-dimensional space. Figures 7 and 8 show the relative position and velocity errors. There is no significant difference between the UKF

and the EKF under this ideal condition. These results indicate that the UKF does not give any advantages in this case.

In the second simulation, errors of −10° in yaw, −15° in pitch and −25° in roll are added to the initial condition attitude estimate using Eq. (54), with the bias estimate set to zero. The initial attitude covariance is set to (20 deg)2, and the initial bias covariance is unchanged. Whereas the EKF never converges, the UKF converges to a value below 0.2° in attitude errors and respective 3σ bounds before one period of the chief as shown in Figs. 9 and 10. The attitude estimated by the EKF is not appropriate in this case.
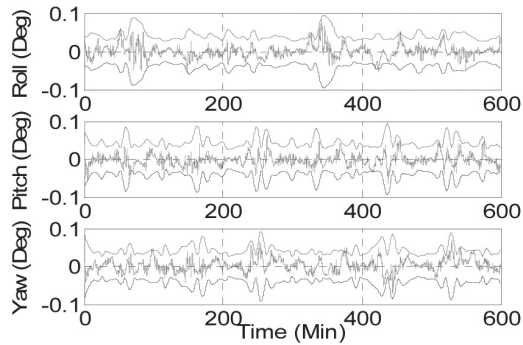
(a) Extended Kalman filter
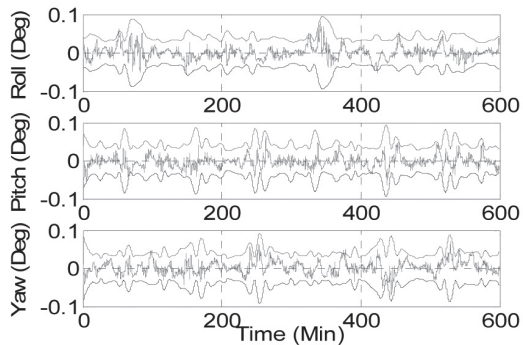
(b) Unscented Kalman filter

Fig. 4. Attitude errors and 3σ bounds.
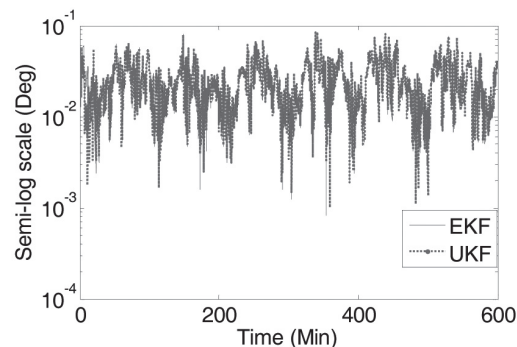
(b) Unscented Kalman filter

Fig. 5. Norm of attitude errors.
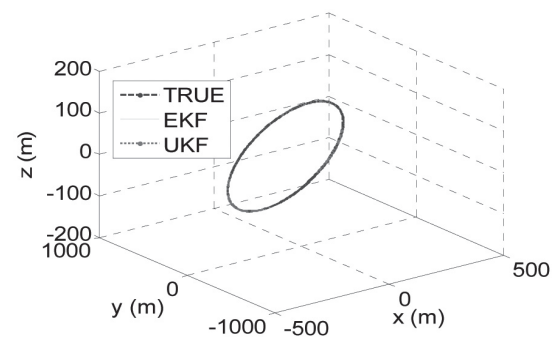
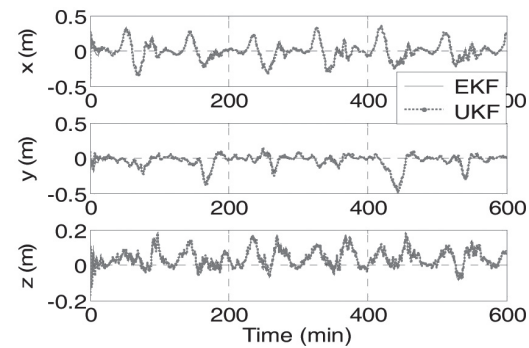Fig. 6. Estimated relative orbit.

Fig. 7. Relative position errors.
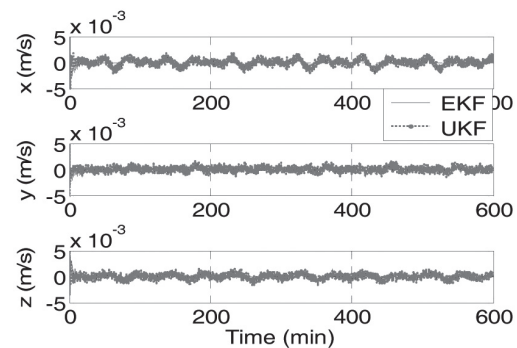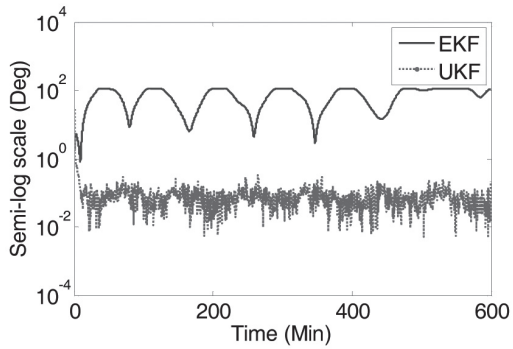

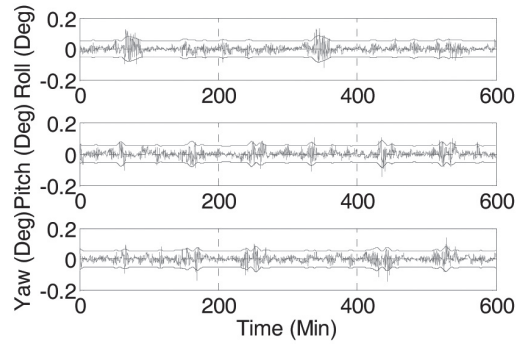Fig. 8. Relative velocity errors.

Fig. 9. Norm of attitude errors.

Fig. 12. Attitude errors and 3σ bounds.

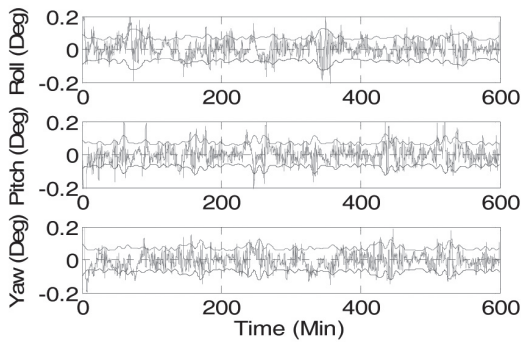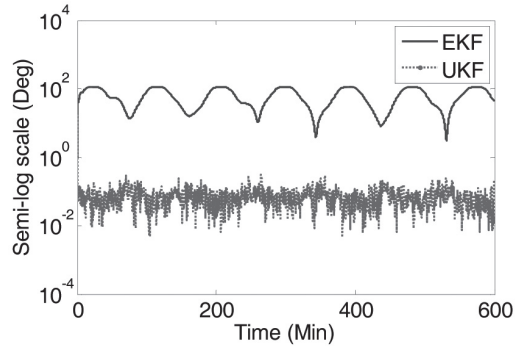
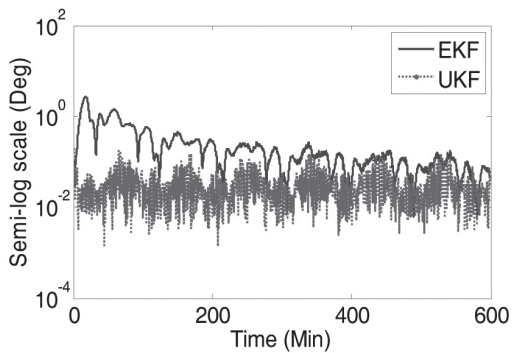Fig. 10. Attitude errors and 3σ bounds.

Fig. 13. Norm of attitude errors.

Fig. 11. Norm of attitude errors.
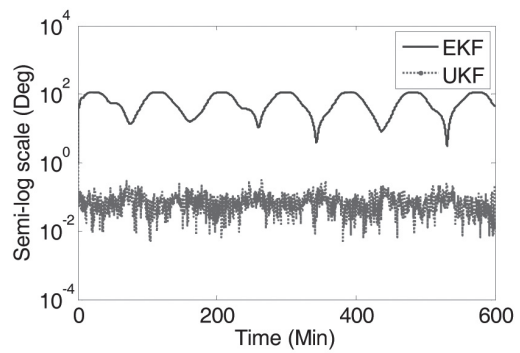

Fig. 14. Attitude errors and 3σ bounds.

In the third simulation, with initial biases set to zero, the initial attitude error is set to zero. Instead, errors of (10 m, −10 m and 10 m) are made in the initial relative position and errors of (0.5 m/s, 0.5 m/s and 0.5 m/s) are made to the relative initial velocity. The EKF takes long time to converge. In addition, it never converges to a value below 0.1° in attitude errors and respective 3σ bounds stably as shown in Fig. 11, whereas the UKF converges to a value near 0.1° from the beginning in Fig. 1

The fourth simulation portrays the most realistic situation. All initial attitude, bias, position, and velocity errors are considered together as in the second and the third simulations. The estimation performance of the EKF deteriorates throughout the simulation, whereas the UKF converges to below 0.2 degrees attitude errors and respective 3σ bounds as shown in Figs. 13 and 14. In all these simulations, the UKF demonstrates its robustness under the initial error conditions.

35

7. Conclusions

This work extended a previously suggested approach for absolute attitude estimation to relative attitude estimation and navigation of spacecrafts based on the use of the UKF, and evaluated the performance of this extended approach for bounded relative motion to verify its robustness under initial error-conditions. This work also employed the quaternion expression, which was represented by a three-dimensional vector of generalized Rodrigues parameters, to maintain a unit quaternion constraint. For estimations of relative attitude, relative position and velocity, the error-state vector was combined. The simulation results using the UKF were compared with those for the EKF. The states estimated by the UKF converged more quickly and precisely with the initial error conditions. The estimated relative position and velocity were validated by comparing them with the state computed from the two orbits generated by HPOP in STK. Thus, the implemented UKF demonstrated its robustness and showed improved estimation results under realistic initial error-conditions. This research shows that the VISNAV system using the UKF can provide precise information on relative attitude, and relative position and velocity under initial error-conditions.

Acknowledgments

References

Analytical Graphics Inc. *Satellite Toolkit*. http://www.agi.com.

Banani, S. A. and Masnadi-Shirazi, M. A. (2007). A new version of unscented Kalman filter. *World Academy of Science, Engineering and Technology*, 26, 192-197.

Brown, R. G. and Hwang, P. Y. C. (1997). *Introduction to Random Signals and Applied Kalman Filtering: with MATLAB Exercises and Solutions*. 3rd ed. New York: Wiley. pp. 202-204.

Cheng, Y., Crassidis, J. L., and Markley, F. L. (2006). Attitude estimation for large field-of-view sensors. *Journal of the Astronautical Sciences*, 54, 433-448.

Cheon, Y. J. and Kim, J. H. (2007). Unscented filtering in a unit quaternion space for spacecraft attitude estimation. *IEEE International Symposium on Industrial Electronics*, Vigo, Spain. pp. 66-71.

Crassidis, J. L. and Markley, F. L. (2003). Unscented filtering for spacecraft attitude estimation. *Journal of Guidance, Control, and Dynamics*, 26, 536-542.

Gaylor, D. and Lightsey, E. G. (2003). GPS/INS Kalman filter design for spacecraft operating in the proximity of the International Space Station. *AIAA Guidance, Navigation, and Control Conference*, Austin, TX. AIAA-2003-5445.

Gunnam, K. K., Hughes, D. C., Junkins, J. L., and Kehtarnavaz, N. (2002). A vision-based DSP embedded navigation sensor. *IEEE Sensors Journal*, 2, 428-441.

Julier, S. J. and Uhlmann, J. K. (2004). Unscented filtering and nonlinear estimation. *Proceedings of the IEEE*, 92, 401-422.

Julier, S. J., Uhlmann, J. K., and Durrant-Whyte, H. F. (1995). New approach for filtering nonlinear systems. P*roceedings of the American Control Conference Seattle*, WA. USA. pp. 1628-1632.

Junkins, J. L., Hughes, D. C., Wazni, K. P., and Pariyapong, V. (1999). Vision-based navigation for rendezvous, docking and proximity operations. *Advances in the Astronautical Sciences*, 101, 203-220.

Kim, S. G., Crassidis, J. L., Cheng, Y., Fosbury, A. M., and Junkins, J. L. (2007). Kalman filtering for relative spacecraft attitude and position estimation. *Journal of Guidance, Control, and Dynamics*, 30, 133-143.

Lefferts, E. J., Markley, F. L., and Shuster, M. D. (1982). Kalman filtering for spacecraft attitude estimation. *Journal of Guidance, Control, and Dynamics*, 5, 417-429.

Schaub, H. and Junkins, J. L. (1996). Stereographic orientation parameters for attitude dynamics: A generalization of the Rodrigues parameters. *Journal of the Astronautical Sciences*, 44, 1-19.

Schaub, H. and Junkins, J. L. (2003). *Analytical Mechanics of Space Systems*. Reston, VA: American Institute of Aeronautics and Astronautics.

Shuster, M. D. (1990). Kalman filtering of spacecraft attitude and the QUEST model. *Journal of the Astronautical Sciences*, 38, 377-393.

Shuster, M. D. (1993). Survey of attitude representations. *Journal of the Astronautical Sciences*, 41, 439-517.

Shuster, M. D. and Oh, S. D. (1981). Three-axis attitude determination from vector observations. *Journal of Guidance and Control*, 4, 70-77.

Van Loan, C. F. (1978). Computing Integrals Involving the matrix exponential. *IEEE Transactions on Automatic Control*, AC-23, 395-404.

VanDyke, M. C., Schwartz, J. L., and Hall, C. D. (2006). Unscented Kalman filtering for spacecraft attitude state and parameter estimation. AAS/AIAA Space Flight Mechanics Meeting, Tampa, FL. pp. 217-228.

Wan, E. A. and Van Der Merwe, R. (2000). The unscented Kalman filter for nonlinear estimation. *Proceedings of IEEE Symposium 2000 on Adaptive Systems for Signal Processing, Communications, and Control Symposium*, Lake Louise, AB, Canada. pp. 153-158.